BELLE2-CONF-PH-2022-002
May 27, 2022

First decay-time-dependent analysis of $B^0 \to K^0\pi^0$ decays at Belle II

(Belle II Collaboration)

Abstract

We report measurements of the branching fraction ($\mathcal{B}$) and direct CP-violating asymmetry ($\mathcal{A}_{CP}$) of the charmless decay $B^0 \to K^0\pi^0$ at Belle II. A sample of e^+e^- collisions, corresponding to $189.8\,\mathrm{fb}^{-1}$ of integrated luminosity, recorded at the $\Upsilon(4S)$ resonance is used for the first Belle II decay-time-dependent analysis of these decays. We reconstruct about 135 signal candidates, and measure $\mathcal{B}(B^0 \to K^0\pi^0) = [11.0 \pm 1.2(\mathrm{stat}) \pm 1.0(\mathrm{syst})] \times 10^{-6}$ and $\mathcal{A}_{CP}(B^0 \to K^0\pi^0) = -0.41^{+0.30}_{-0.32}(\mathrm{stat}) \pm 0.08(\mathrm{syst})$.

1. INTRODUCTION

The $B^0 \to K^0\pi^0$ decay is mediated by flavour-changing neutral currents. In the standard model (SM), the dominant decay amplitude is given by the $b \to sd\overline{d}$ loop, which is dominated by the top quark contribution and carries a weak phase $\arg(V_{tb}V_{ts}^*)$. Here, V_{ij} denote the CKM matrix elements. Such processes are suppressed in the SM and provide an indirect route to search for beyond-the-SM particles that might be exchanged in the loop. In the $B^0 \to K^0\pi^0$ decay, CP violation can occur either directly in the decay amplitude ($\mathcal{A}_{CP}$) or via the interference between decays with and without B^0–$\overline{B}^0$ mixing ($\mathcal{S}_{CP}$). Neglecting subleading contributions to the amplitude, $\mathcal{S}_{CP}$ is expected to be equal to $\sin 2\beta$ and $\mathcal{A}_{CP} \approx 0$, where $\beta \equiv \arg(-V_{cd}V_{cb}^*/V_{td}V_{tb}^*)$. Deviations from these expectations could be due to larger-than-expected subleading SM contributions or by non-SM physics.

Combining measurements from Belle and BaBar [1, 2], particle data group find $\mathcal{A}_{CP}(B^0 \to K^0\pi^0)$ to be consistent with zero within 13% precision. This uncertainty is limiting the overall precision of a sum rule that combines B-meson lifetimes (τ) with branching fractions ($\mathcal{B}$) and CP asymmetries of four $B \to K\pi$ decays, related by isospin symmetry. The sum rule,

$$I_{K\pi} = \mathcal{A}_{CP}(K^+\pi^-) + \mathcal{A}_{CP}(K^0\pi^+)\frac{\mathcal{B}(K^0\pi^+)}{\mathcal{B}(K^+\pi^-)}\frac{\tau_{B^0}}{\tau_{B^+}} \qquad (1)$$

$$-2\mathcal{A}_{CP}(K^+\pi^0)\frac{\mathcal{B}(K^+\pi^0)}{\mathcal{B}(K^+\pi^-)}\frac{\tau_{B^0}}{\tau_{B^+}} - 2\mathcal{A}_{CP}(K^0\pi^0)\frac{\mathcal{B}(K^0\pi^0)}{\mathcal{B}(K^+\pi^-)} = 0,$$

is expected to hold with an uncertainty below 1% and provides an important consistency test of the SM [3]. Deviations from the isospin sum rule can indicate contributions of non-SM physics in the loops, or enhancements of color suppressed SM tree amplitudes. The current measurement of $I_{K\pi}$ value is 0.03 ± 0.08 [4]. The dominant uncertainty on $I_{K\pi}$ sensitivity comes from the uncertainty of $\mathcal{A}_{CP}(K^0\pi^0)$. Therefore a precise measurement of $\mathcal{A}_{CP}(K^0\pi^0)$ is very important for the consistency test of SM.

Preliminary results on $\mathcal{B}$ and $\mathcal{A}_{CP}$ of $B^0 \to K^0\pi^0$ decays have been reported by Belle II using a data sample corresponding to $62.8\,\mathrm{fb}^{-1}$. In this analysis, we extend over those measurements by using a larger sample ($189.8\,\mathrm{fb}^{-1}$) complemented by a decay-time-dependent analysis that enhances our sensitivity to $\mathcal{A}_{CP}$.

At Belle II, pairs of neutral B mesons are coherently produced in the process $e^+e^- \to \Upsilon(4S) \to B^0\overline{B}^0$. When one of the B mesons decays to a CP eigenstate f_{CP}, such as $K_S^0\pi^0$, and the other to a flavor-specific final state f_{tag}, the time-dependent decay rate is given by

$$\mathcal{P}(\Delta t) = \frac{e^{-|\Delta t|/\tau_{B^0}}}{4\tau_{B^0}}[1 + q\{\mathcal{A}_{CP}\cos(\Delta m_d \Delta t) + \mathcal{S}_{CP}\sin(\Delta m_d \Delta t)\}], \qquad (2)$$

where $\Delta t = t_{CP} - t_{\mathrm{tag}}$ is the proper time difference between the decays into f_{CP} and f_{tag}, q equals $+1$ (-1) for the B^0 ($\overline{B}^0$) decay to f_{tag}, and Δm_d is the B^0–$\overline{B}^0$ mixing frequency. The key challenge for this analysis is to find the CP side vertex position, for that K_S^0-flight direction is project back to the interaction region and put a criteria on K_S^0 to decay inside the vertex detector. The signal yield and CP asymmetry are obtained from a four-dimensional fit. The full analysis is developed and tested with simulation, and validated with data samples in control decay before inspecting on data to measure the physics observables. Due to the limited sensitivity provided by the available data sample, we measure $\mathcal{A}_{CP}$ by fixing $\mathcal{S}_{CP}$, Δm_d and τ_{B^0} to their known values [5].

2. THE BELLE II DETECTOR AND DATA SAMPLE

Belle II [6] is a particle spectrometer having almost 4π solid-angle coverage, designed to reconstruct final-state particles of e^+e^- collisions delivered by the SuperKEKB asymmetric-energy collider [7]. It is located at the KEK laboratory in Tsukuba, Japan. The energies of the positron and electron beams are 4 and 7 GeV, respectively. Belle II comprises a number of subdetectors surrounding the interaction region in a cylindrical geometry. The innermost one is the vertex detector (VXD), which uses position-sensitive silicon layers to sample the trajectories of charged particles ('tracks') in the vicinity of the interaction region to determine the decay positions of their long-lived parent particles. The VXD includes two inner layers of pixel sensors and four outer layers of double-sided microstrip sensors. The second pixel layer is currently incomplete covering one sixth of the azimuthal angle. Charged-particle momenta and charges are measured by a large-radius, small-cell, helium-ethane central drift chamber (CDC), which also offers particle-identification information via a measurement of specific ionization. A Cherenkov-light angle and time-of-propagation detector surrounding the CDC provides charged-particle identification in the central detector volume, supplemented by proximity-focusing, aerogel, ring-imaging Cherenkov detectors in the forward region with respect to the electron beam. A CsI(Tl)-crystal electromagnetic calorimeter (ECL) provides energy measurements of electrons and photons. A solenoid surrounding the ECL generates a uniform axial 1.5 T magnetic field filling its inner volume. Layers of plastic scintillators and resistive-plate chambers, interspersed between the magnetic flux-return iron plates, allow for the identification of K_L^0 mesons and muons. The subdetectors most relevant for our study are the VXD, CDC, and ECL.

We use all good quality collision data collected, at a center-of-mass (CM) energy near the $\Upsilon(4S)$ resonance, corresponding to an integrated luminosity of $189.8\,\text{fb}^{-1}$. We use large samples of simulated $e^+e^- \to q\overline{q}$ ($q = u, d, s, c$), $\Upsilon(4S) \to B^0\overline{B}^0$ and B^+B^- events to optimize the event selection and study possible background contributions. We also use simulated signal events to determine signal models and estimate the selection efficiency. The B-meson decays are simulated using the EvtGen generator [8], with the effect of final-state radiation incorporated via the Photos package [9]. The simulation of $e^+e^- \to q\overline{q}$ continuum background uses the KKMC generator [10] interfaced to Pythia [11]. The interactions of final-state particles with the detector are simulated using Geant4 [12].

3. RECONSTRUCTION AND SELECTION

Tracks are reconstructed with the VXD and CDC. Photons are identified as isolated ECL clusters that are not matched to any track. Candidates K_S^0 are reconstructed from pairs of opposite charged particles with dipion mass between 482 and 513 MeV/c^2. We reconstruct π^0 candidates from pairs of photons that have energies greater than 80 (223) MeV if detected in the barrel (endcap) ECL. We apply different energy thresholds between barrel and endcap to suppress beam background, which is higher in the endcap compared to barrel region. The selection also requires the diphoton mass to lie between 119 and 150 MeV/c^2 and the absolute cosine of its helicity angle to be less than 0.953. These criteria suppress contributions from misreconstructed π^0 candidates.

The B-meson candidate is reconstructed by combining a K_S^0 with a π^0 candidate. For this purpose, we use two kinematic variables, the beam-energy-constrained mass (M_{bc}) and the energy difference (ΔE),

$$\begin{aligned} M_{\rm bc} &= \sqrt{E_{\rm beam}^2 - \vec{p}_B^{\,2}}, \\ \Delta E &= E_B - E_{\rm beam}, \end{aligned} \tag{3}$$

where $E_{\rm beam}$ is the beam energy, and E_B and $\vec{p}_B$ are respectively the reconstructed energy and momentum of the B meson; all calculated in the CM frame.

The presence of a high momentum π^0 causes a nontrivial correlation between $M_{\rm bc}$ and ΔE due to the shower leakage of final-state photons. To reduce the correlation with ΔE, we use a modified version of $M_{\rm bc}$ that is defined in terms of the beam energy and momenta of final-state particles as

$$M'_{\rm bc} = \sqrt{E_{\rm beam}^2 - \left(\vec{p}_{K_S^0} + \frac{\vec{p}_{\pi^0}}{|\vec{p}_{\pi^0}|}\sqrt{(E_{\rm beam} - E_{K_S^0})^2 - m_{\pi^0}^2}\right)^2}, \tag{4}$$

where all kinematic quantities are again calculated in the CM frame. We retain candidate events satisfying $5.24 < M'_{\rm bc} < 5.29\ \text{GeV}/c^2$ and $|\Delta E| < 0.30\ \text{GeV}$.

To measure the proper time difference Δt, we determine the signal and tag-side B decay vertices. The signal B vertex is obtained by projecting the flight direction of the K_S^0 candidate back to the interaction region. The K_S^0 flight direction is determined from its decay vertex and momentum. The intersection of the K_S^0-flight projection with the interaction region provides a good approximation of the signal B decay vertex, since both the transverse flight length of the B^0 meson and the transverse size of the interaction region are small compared to the B^0 flight length along the boost direction. The tag-side vertex is obtained with tracks that are not associated to the $B^0 \to K_S^0\pi^0$ decay. We obtain the Δt value by dividing the longitudinal distance between signal and tag vertices by the speed of light and the Lorentz boost of the $\Upsilon(4S)$ system in the lab frame. Signal candidates with poorly measured Δt, mainly due to K_S^0 mesons decaying outside of the VXD acceptance, are suppressed by requiring the estimated uncertainty on Δt to be below 2.5 ps. This requirement removes about 50% of signal candidates, which contribute negligible information for the decay-time-dependent analysis.

Events from continuum $e^+e^- \to q\bar{q}$ production are suppressed using a boosted-decision-tree (BDT) classifier [13] that exploits 39 event-topology variables known to have discrimination between B-meson signal and continuum background. The following variables are those offering most discrimination between signal and continuum: modified Fox-Wolfram moments [14], CLEO cones [15], the magnitude of thrust axis for the reconstructed B candidate and the cosine of the angle between the thrust axis of signal B and that of rest of events. The BDT is trained on samples of simulated $e^+e^- \to q\bar{q}$, $B^0\overline{B}^0$ and B^+B^- events, each equivalent to an integrated luminosity of 1 ab^{-1}. The BDT output distribution ($C_{\rm out}$) is shown in Fig. 1. We applied the $C_{\rm out} = 0.60$ criterion and reject about 89% of the continuum background with a 18% relative loss in signal efficiency. We translate it into a new variable,

$$C'_{\rm out} = \ln\left(\frac{C_{\rm out} - C_{\rm out,min}}{C_{\rm out,max} - C_{\rm out}}\right), \tag{5}$$

which is conveniently parametrized with Gaussian functions. Here, $C_{\rm out,min} = 0.60$ and $C_{\rm out,max} = 0.99$.

After the final selection and background suppression, the average number of B candidates per event is 1.009. The multiple candidates arise due to a random combination of final-state

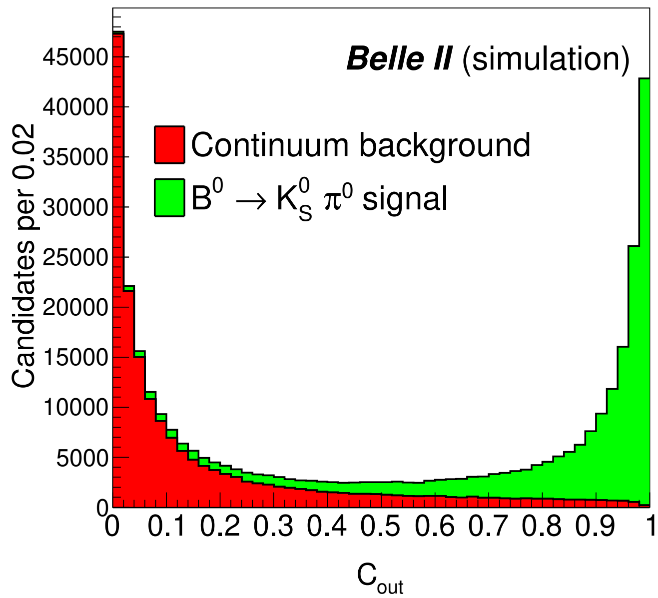

FIG. 1. Distributions of the BDT output $C_{\rm out}$ for simulated signal and $e^+e^- \to q\overline{q}$ events.

particles. To select the best one in an event with multiple candidates, we first compare the π^0 mass-constrained fit χ^2 probability ('p-value'). If there are more than one candidates sharing the same p-value, we choose the one with the best p-value of the fit of the K_S^0 vertex; this is the fit of the decay-chain of the candidate. This selection retains the correct B candidate in 74% of our simulated events.

The signal efficiency (ϵ) of correctly reconstructed events after all the selection is 12.3%. From simulation we find that signal candidates can be incorrectly reconstructed in 1.5% of the times by accidentally selecting a particle from the other B meson decay. We consider those candidates as part of the signal.

We determine the flavor of the tag-side B meson (q) from properties of final-state particles that are not associated with the reconstructed $B^0 \to K_S^0\pi^0$ decay. The Belle II flavor tagging algorithm [16] returns, as the tagging decision, q and the tagging dilution, r, that ranges from 0 (no flavor discrimination) to 1 (unambiguous flavor assignment). Multivariate category-based flavor-tagger algorithm uses the information of B-decay products to determine the quark-flavor of B mesons.

4. DETERMINATION OF BRANCHING FRACTION AND *CP* ASYMMETRY

We obtain the signal yield and CP asymmetry from a four-dimensional extended maximum-likelihood fit to the unbinned distributions of $M'_{\rm bc}$, ΔE, $C'_{\rm out}$, and Δt. For the signal component, $M'_{\rm bc}$ is modeled with the sum of a Crystal Ball [17] and a Gaussian function with a common mean; ΔE with the sum of a Crystal Ball and a double Gaussian function, all three with a common mean; and $C'_{\rm out}$ with the sum of an asymmetric and a regular Gaussian function. Its Δt probability density function (PDF) is given by

$$\mathcal{P}_{\rm sig}(\Delta t, q) = \frac{\mathrm{e}^{-|\Delta t|/\tau_{B^0}}}{4\tau_{B^0}}[\{1 - q\Delta w_r + q\mu_r(1-2w_r)\} + \{q(1-2w_r) + \mu_r(1-q\Delta w_r)\} \\ \{\mathcal{A}_{CP}\cos(\Delta m_d \Delta t) + \mathcal{S}_{CP}\sin(\Delta m_d \Delta t)\}] \otimes \mathcal{R}_{\rm sig}, \quad (6)$$

where w_r is the fraction of wrongly tagged events, Δw_r is the difference in w_r between B^0 and $\overline{B}^0$, μ_r is the difference in their tagging efficiency corresponds to the fraction of events to which a flavor tag can be assigned, and $\mathcal{R}_{\rm sig}$ is the Δt resolution function, composed of the sum of two Gaussians with width $\approx 0.9\,$ps which is parametrized from simulated events. We set τ_{B^0} to $1.520\,$ps, Δm_d to $0.507\,{\rm ps}^{-1}$, and $\mathcal{S}_{CP}$ to 0.57 [5]. The data are divided into seven $q \cdot r$ bins with the tagging parameters for each bin (w_r, Δw_r, and μ_r) fixed to the respective values obtained in Ref. [16]. The effective tagging efficiency, w_r and μ_r are $(30.0 \pm 1.2)\%$, (2–47)% and (0.5–11)%, respectively. All signal PDF shapes are fixed to the values determined from a $q \cdot r$ binned fit to simulated signal events.

For the continuum background component, an ARGUS function [18] is used for $M'_{\rm bc}$, a linear function for ΔE, and the sum of an asymmetric and a regular Gaussian function for $C'_{\rm out}$. Its Δt distribution is modeled with an exponential function convolved with a Gaussian for the tail; we use a double Gaussian for its resolution function ($\mathcal{R}_{q\overline{q}}$). For the continuum background component, we float the PDF shape parameters, which are found to be independent of the $q \cdot r$ bins. For the $B\overline{B}$ background component, a two-dimensional Kernel estimation PDF [19] is used to model the ΔE vs. $M'_{\rm bc}$ distribution, and the sum of an asymmetric and a regular Gaussian function is used for $C'_{\rm out}$. Its Δt distribution is modeled with an exponential function convolved with a Gaussian for the tail; we again use a double Gaussian for its resolution function ($\mathcal{R}_{B\overline{B}}$). The $B\overline{B}$ background shape parameters are fixed from a fit to the corresponding simulated sample.

The fit parameters are the signal yield $N_{\rm sig}$; $\mathcal{A}_{CP}$; $B\overline{B}$ background yield, which is Gaussian constrained to the result of a fit to the ΔE sideband in data; continuum background yield; $M'_{\rm bc}$ ARGUS parameter; ΔE slope; and $C'_{\rm out}$ relative width for the $q\overline{q}$ component. We correct the signal $M'_{\rm bc}$, ΔE, and $C'_{\rm out}$ PDF shapes for possible data–simulation differences, according to the values obtained with a control sample of $B^+ \to \overline{D}^0(\to K^+\pi^-\pi^0)\pi^+$ (charge conjugated modes are implicitly included hereafter). In order to mimic the signal decay, we use the similar π^0 selection. We use a maximum-likelihood fit to the unbinned distribution of $M'_{\rm bc}$, ΔE, and $C'_{\rm out}$, using PDF shapes similar to that employed in the fit to signal data. We use a control sample of $B^0 \to J/\psi(\to \mu^+\mu^-)K^0_S$ decays to validate the time-dependent analysis. To mimic the signal decay, we do not use the two muons coming from the J/ψ decay to reconstruct the signal B decay vertex. We use a maximum-likelihood fit to the unbinned distributions of $M_{\rm bc}$ and Δt, using PDF shapes and resolution functions similar to those employed in the fit to signal data. The B^0 lifetime and $\mathcal{A}_{CP}$ are measured to be $1.59^{+0.09}_{-0.08}\,$ps and -0.03 ± 0.10, respectively, which are consistent with their known values [5]. This provides convincing data-driven support to the time-dependent part of the analysis. The same sample is also used to correct the Δt PDF shape parameters for possible data–simulation differences. The estimator properties (bias, uncertainties) have been thoroughly studied in simplified and realistic simulated experiments and found to be as expected.

Figure 2 shows the four projections of the fit to the seven $q \cdot r$-integrated data sample. For each projection the signal enhancing criteria, defined by $5.27 < M'_{\rm bc} < 5.29\,{\rm GeV}/c^2$, $-0.15 < \Delta E < 0.10\,$GeV, $|\Delta t| < 10.0\,$ps, and $C'_{\rm out} > 0.0$, are applied on all but for the variable displayed. The obtained signal yield is 135^{+16}_{-15}, where the quoted uncertainty is statistical only. We also find 2214^{+49}_{-48} continuum and 44 ± 5 $B\overline{B}$ background events. We determine the branching fraction using the following formula:

$$\mathcal{B}(B^0 \to K^0\pi^0) = \frac{N_{\rm sig}}{2 \times N_{B\overline{B}} \times f^{00} \times \epsilon \times \mathcal{B}_s}, \tag{7}$$

where $N_{B\overline{B}} = (197.2 \pm 5.70) \times 10^6$, $f^{00} = 0.487 \pm 0.010$, and $\mathcal{B}_s = 0.5$ are the number of $B\overline{B}$ pairs, $\Upsilon(4S) \to B^0\overline{B}^0$ branching fraction, and $K^0 \to K^0_S \to \pi^+\pi^-$ branching fraction, respectively. The $B^0 \to K^0\pi^0$ branching fraction and direct CP asymmetry are measured to be $(11.0 \pm 1.2 \pm 1.0) \times 10^{-6}$ and $0.41^{+0.30}_{-0.32} \pm 0.08$, respectively. The first uncertainties are statistical and the second are systematic (described in Section 5). This extends the previous measurement [20] of $\mathcal{B}$ and $\mathcal{A}_{CP}$ in $B^0 \to K^0\pi^0$ decays, where no information on the proper time difference had been used.

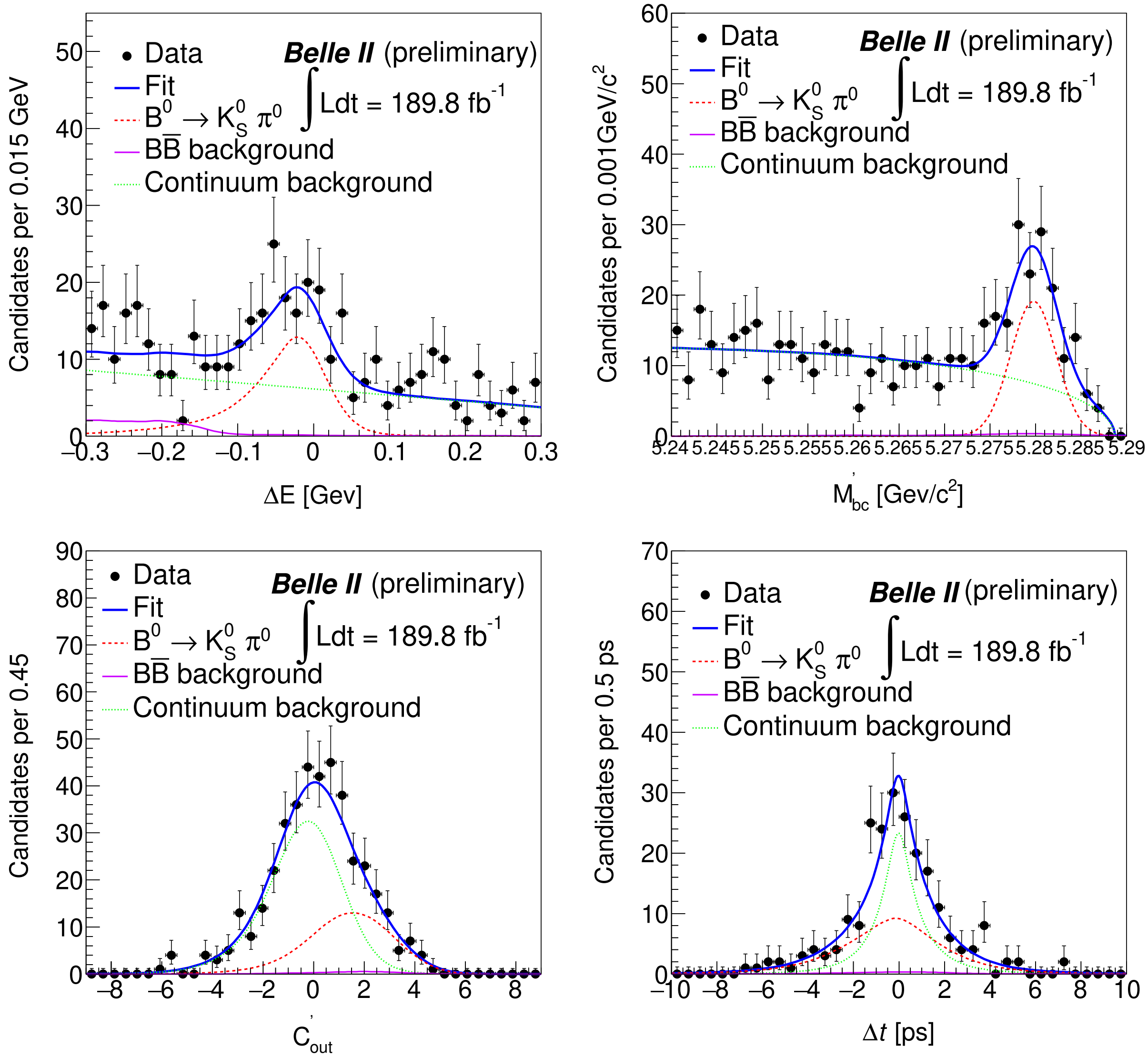

FIG. 2. Signal enhanced fit projections of ΔE (top-left), $M'_{\rm bc}$ (top-right), $C'_{\rm out}$ (bottom-left), and Δt (bottom-rigt) shown for the sample integrated in the seven $q \cdot r$ bins.

5. SYSTEMATIC UNCERTAINTIES

Various systematic uncertainties contributing to $\mathcal{B}$ and $\mathcal{A}_{CP}$ are listed in Table I. Assuming these sources to be independent, we add their contributions in quadrature to get the total systematic uncertainty. The systematic uncertainty due to possible differences between data and simulation in the reconstruction of charged particles is 0.3% per track [21]. We linearly add this uncertainty corresponding to each of the two pion tracks coming from the K_S^0 decay in the signal side. From a comparison of the K_S^0 yield in data and simulation, we find that the ratio of K_S^0 reconstruction efficiency changes approximately linearly as a function of its flight length [21]. We apply an uncertainty of 0.4% for each centimeter of the average flight length of K_S^0 candidates resulting in a 4.2% total systematic uncertainty to $\mathcal{B}$. We estimate the systematic uncertainty due to possible differences between data and simulation in the π^0 reconstruction and selection by comparing the inclusive decay sample of $D^0 \to K^-\pi^+\pi^0$ with $D^0 \to K^-\pi^+$ [22]. The data–simulation efficiency ratio is found to be close to unity with an uncertainty of 7.5%, which we assign as the systematic uncertainty to $\mathcal{B}$. We evaluate possible data–simulation differences in the continuum-suppression efficiency using the control sample of $B^+ \to \overline{D}^0(\to K^+\pi^-\pi^0)\pi^+$. As the ratio of efficiencies obtained in data and simulation is close to unity, the statistical uncertainty on the ratio (1.6%) is assigned as a systematic uncertainty to $\mathcal{B}$. We estimate the systematic uncertainty on $\mathcal{A}_{CP}$ due to wrong tag fraction by varying the parameter individually for each $q\cdot r$ region by its 1σ uncertainty. The systematic uncertainty due to resolution function is estimated in a similar fashion. As external inputs τ_{B^0}, Δm_d, and $\mathcal{S}_{CP}$ are fixed to their known values in the fit, the associated systematic uncertainty is estimated by varying their values by $\pm 1\sigma$. In the nominal fit, we assume the $B\overline{B}$-background decays to be CP symmetric. However, there could be a nontrivial asymmetry arising due to this component. To take such possibility into account, we use an alternative Δt PDF given by

$$\mathcal{P}_{B\bar{B}}(\Delta t, q) = \frac{e^{-|\Delta t|/\tau_{B^0}}}{4\tau_{B^0}}[1 + q\{\mathcal{A}'_{CP}\cos(\Delta m_d \Delta t) + \mathcal{S}'_{CP}\sin(\Delta m_d \Delta t)\}] \otimes R_{B\bar{B}}. \tag{8}$$

We perform two different fits by setting $\mathcal{S}'_{CP}$ to either $+1$ or -1, and $\mathcal{A}'_{CP} = 0.0$. We then calculate the deviations in signal $\mathcal{A}_{CP}$ from its nominal value. These deviations are assigned as a systematic uncertainty to $\mathcal{A}_{CP}$ due to $B\overline{B}$ background asymmetry. An overall uncertainty of 3.2% on $\mathcal{B}$ is taken as a systematic uncertainty due to the number of $B\overline{B}$ pairs used, which includes the uncertainty on f^{00}, cross section, integrated luminosity, and possible shifts from the peak CM energy as a function of time. The uncertainties due to signal PDF shape parameters are estimated by varying their correction factors by $\pm 1\sigma$, where σ denote the corresponding statistical uncertainties. Similarly, the uncertainties due to background PDF shape are calculated by varying all fixed parameters by $\pm 1\sigma$, determined from the fit to simulated samples. We fix the $M'_{\rm bc}$ ARGUS endpoint to the value obtained from a fit to the sideband data. Subsequently we vary it by $\pm 1\sigma$ to assign a systematic uncertainty, where σ is the uncertainty from the fit. Potential fit bias is checked by performing an ensemble test comprising 1000 simplified simulated experiments in which signal events are drawn from the corresponding simulation sample and background events are generated according to their PDF shapes. We calculate the mean shift of signal yield from the input value and assign it as a systematic uncertainty. The tag-side flavor is determined from flavor-specific final states but there exist some flavor nonspecific channels. For example, the flavor-specific $\overline{B}^0 \to D^+\pi^-$ is a CKM-favoured channel, whose suppressed counterpart $B^0 \to D^+\pi^-$ may exist on the tag side. As a result, there can be CP violation on the tag side. The systematic uncertainty on $\mathcal{A}_{CP}$ arising due to unaccounted for tag-side interference is taken from Ref. [23]. A possible systematic uncertainty related to VXD misalignment is neglected in this study.

TABLE I. List of systematic uncertainties contributing to the branching fraction and direct CP asymmetry.

Source	$\delta\mathcal{B}$ (%)	$\delta\mathcal{A}_{CP}$
Tracking efficiency	0.6	–
K_S^0 reconstruction efficiency	4.2	–
π^0 reconstruction efficiency	7.5	–
Continuum suppression efficiency	1.6	–
Number of $B\overline{B}$ pairs	3.2	–
Flavor tagging	–	0.040
Resolution function	–	0.050
External inputs	0.4	0.021
$B\overline{B}$ background asymmetry	–	0.002
Signal modelling	1.0	0.015
Background modelling	0.9	0.004
Possible fit bias	2.0	0.010
Tag-side interference	–	0.038
Total	9.6	0.086

6. SUMMARY

We report measurements of the branching fraction and direct CP asymmetry in $B^0 \to K^0\pi^0$ decays using a data sample, corresponding to $189.8\,\text{fb}^{-1}$ of integrated luminosity, recorded by Belle II at the $\Upsilon(4S)$ resonance. The observed signal yield is 135^{+16}_{-15}. We measure $\mathcal{B}(B^0 \to K^0\pi^0) = [11.0\pm1.2(\text{stat})\pm1.0(\text{syst})]\times10^{-6}$ and $\mathcal{A}_{CP} = -0.41^{+0.30}_{-0.32}(\text{stat})\pm0.08(\text{syst})$. This is the first measurement of $\mathcal{A}_{CP}$ in $B^0 \to K^0\pi^0$ performed at Belle II using a decay-time-dependent analysis. The results agree with previous determinations [5, 20].

7. ACKNOWLEDGEMENT

We thank the SuperKEKB group for the excellent operation of the accelerator; the KEK cryogenics group for the efficient operation of the solenoid; and the KEK computer group for on-site computing support.

[1] M. Fujikawa et al. (Belle Collaboration), Phys. Rev. D **81**, 011101 (2010).
[2] B. Aubert et al. (BaBar Collaboration), Phys. Rev. D. **79**, 052003 (2009).
[3] M. Gronau, Phys. Lett. B **627**, 82 (2005).

[4] T. Gershon and A. Soni, J. Phys. G **33** (2007) 479–492.

[5] Y. Amhis et al. (Heavy Flavor Averaging Group), Eur. Phys. J. C (2021) 81:226, arXiv:1909.12524.

[6] T. Abe et al. (Belle II Collaboration), KEK Report 2010-1, arXiv:1011.0352.

[7] K. Akai, K. Furukawa, and H. Koiso (SuperKEKB Group), Nucl. Instrum. Meth. A **907**, 188 (2018).

[8] D. Lange, Nucl. Instrum. Meth. A **462**, 152 (2001).

[9] E. Barberio, B. van Eijk, and Z. Was, Comp. Phys. Comm. **66**, 115 (1991).

[10] B. Ward, S. Jadach, and Z. Was, Nucl. Phys. B Proc. Suppl. **116**, 73 (2003)

[11] T. Sjöstrand, S. Mrenna, and P. Skands, Comp. Phys. Comm. **178**, 852 (2008).

[12] S. Agostinelli et al. (GEANT4 Collaboration), Nucl. Instrum. Meth. A **506**, 250 (2003).

[13] T. Keck, arXiv:1609.06119.

[14] G. C. Fox and S. Wolfram, Phys. Rev. Lett. **41**, 1581 (1978).

[15] D. M. Asner et al. (CLEO Collaboration), Phys. Rev. D 53, 1039 (1996).

[16] F. Abudinén et al. (Belle II Collaboration), Eur. Phys. J. C **82**, 283 (2022).

[17] T. Skwarnicki, PhD thesis, INP Krakow, DESY-F31-86-02 (1986).

[18] H. Albrecht et al. (ARGUS Collaboration), Phys. Lett. B **241**, 278 (1990).

[19] K. S. Cranmer, Comp. Phys. Comm. **136**, 198 (2001).

[20] F. Abudinén et al. (Belle II Collaboration), BELLE2-CONF-PH-2021-001, arXiv:2104.14871.

[21] V. Bertacchi et al. (Belle II Tracking Group), Comp. Phys. Comm. **259**, 107610 (2021).

[22] G. Bonvicini et al. (CLEO Collaboration), Phys. Rev. D **89**, 072002 (2014).

[23] I. Adachi et al. (Belle Collaboration), Phys. Rev. Lett. **108**, 171802 (2012).

[24] L. Šantelj et al. (Belle Collaboration), JHEP **10**, 165 (2014).